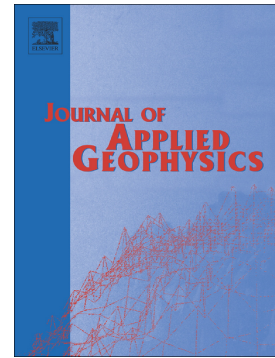


Journal Pre-proof

Permeability prediction using logging data from tight reservoirs based on deep neural networks

Zhijian Fang, Jing Ba, José M. Carcione, Fansheng Xiong, Li Gao



PII: S0926-9851(24)00217-9

DOI: <https://doi.org/10.1016/j.jappgeo.2024.105501>

Reference: APPGEO 105501

To appear in: *Journal of Applied Geophysics*

Received date: 13 June 2024

Revised date: 18 August 2024

Accepted date: 26 August 2024

Please cite this article as: Z. Fang, J. Ba, J.M. Carcione, et al., Permeability prediction using logging data from tight reservoirs based on deep neural networks, *Journal of Applied Geophysics* (2024), <https://doi.org/10.1016/j.jappgeo.2024.105501>

This is a PDF file of an article that has undergone enhancements after acceptance, such as the addition of a cover page and metadata, and formatting for readability, but it is not yet the definitive version of record. This version will undergo additional copyediting, typesetting and review before it is published in its final form, but we are providing this version to give early visibility of the article. Please note that, during the production process, errors may be discovered which could affect the content, and all legal disclaimers that apply to the journal pertain.

© 2024 Published by Elsevier B.V.

Permeability prediction using logging data from tight reservoirs based on deep neural networks

Zhijian Fang^a, Jing Ba^{a,*}, José M Carcione^{a,b}, Fansheng Xiong^c, Li Gao^a

^a*School of Earth Sciences and Engineering, Hohai University, Nanjing 211100, China*

^b*National Institute of Oceanography and Applied Geophysics - OGS, Trieste 34010, Italy*

^c*Beijing Institute of Mathematical Sciences and Applications, Beijing 101408, China*

ABSTRACT

Permeability is a critical parameter for evaluating reservoir properties, and accurate prediction is an important basis for identifying high-quality reservoirs and geological modeling. However, the strong heterogeneity, complex lithology and diagenesis in the reservoirs of this region pose a major challenge for the accurate assessment of reservoir permeability. In recent years, the use of machine learning (ML) to solve problems in geophysical well logging and related fields has gained much attention thanks to advances in data science and artificial intelligence. ML is any predictive algorithm or combination of algorithms that learns from data and makes predictions without being explicitly coded with a deterministic model. The most immediate example is deep neural networks (DNN) that are trained with data to minimize a cost function and make predictions. The tight reservoirs in the Chang 7 Member of the Ordos Basin host significant oil and gas resources and have recently emerged as the main focus of unconventional oil and gas exploration and development. In this work, we performed DNN-based permeability prediction for the tight reservoirs in the Ordos Basin area. From 19 well logs, we selected effective data points from 17 wells for DNN training after preprocessing and used the remaining two wells for testing. First, we trained the DNN with all collected parameters as

inputs, resulting in permeability prediction R^2 values of 0.64 and 0.72 for the two wells, indicating a good fit. We then optimized the input parameters by performing a crossplot analysis between these parameters and the permeability. Using the same network structure (with all hyperparameters set the same), we trained the DNN again to obtain a new DNN-based model. The prediction results showed that removing input parameters with poor correlation to permeability improved the prediction accuracy with R^2 values of 0.70 and 0.87 for the two wells.

Keywords: Permeability prediction; well-log data; machine learning; deep neural networks; Ordos Basin; tight reservoirs

1. Introduction

New geophysical exploration technologies are expected to provide information not only on the presence and saturation of geofluids (e.g. geologically stored CO_2 and H_2 , etc.) in the reservoirs, but also information on whether the geofluid can flow so that it can be exploited (Guo and Gurevich, 2020; Guo et al., 2022; Ba et al., 2023a; Guo et al., 2023; Carcione et al., 2023; Lu et al., 2023). A key parameter that determines the flowability of geofluid is the permeability of the reservoir rock (Carcione et al., 2018, 2019; Guo et al., 2019; Guo et al., 2022a, b). Establishing a quantitative relationship between permeability and the petrophysical properties of the reservoir at log and seismic frequencies is crucial for efficient recovery of oil and gas resources (Ahmed et al., 1991).

The permeability at well locations is primarily determined from core samples or logging data. Laboratory measurements of permeability using drill core samples (He et al., 2020; An et al., 2023; Ba et al., 2023b) are very accurate but time-consuming and costly. Methods based on rock physics theories and multiple logs to fit permeability have improved efficiency and reduced costs to some extent. Rock physics models used for permeability prediction include the Archie equation (Archie,

1941), the Kozeny-Carman model (Carman, 1961), the Timur model (Timur, 1968) and various improved models (Carcione et al., 2010; Srisutthiyakorn and Mavko, 2017; Madadi and Müller, 2019; Xiong et al., 2020; Zhang et al., 2023). The accuracy of permeability estimation by different models depends on factors such as their representation of actual conditions, the selection of log sensitive parameters and optimal parameter combinations. However, existing rock physics models are often based on numerous assumptions, which makes it difficult to effectively simulate the physical mechanisms of complex oil and gas reservoirs and leads to discrepancies between the predicted and actual permeability.

In recent years, the use of machine learning (ML) to solve problems in geophysical well logging, seismic exploration, and related fields has gained much attention with the advances in data science and artificial intelligence (Anemangely et al., 2017; Botterill and McMillan, 2023). In contrast to conventional methods, data-driven ML approaches go beyond domain-specific knowledge, offer a new perspective on data and explore larger functional spaces. By mapping data and targets in situations where physical relationships are unknown, these methods provide a means to characterize relationships between variables in high-dimensional spaces, reducing the need for researchers to have extensive knowledge of geology, geophysics, and rock physics (Bergen et al., 2019). In particular, various ML technologies have been used for reservoir permeability prediction, e.g., backpropagation (BP) neural networks, k-nearest neighbor (KNN) regression, extreme gradient boosting (XGBoost) regression, decision tree (DT) regression, and random forest (RF) regression (Helle et al., 2001; Jamshidian et al., 2015; Zhao et al., 2022), etc. Most of these methods have proven to be reliable prediction methods. However, they provide unsatisfactory predictions for heterogeneous reservoirs,

especially in the case of limited logging data (Huang et al., 1996. Helle et al., 2001; Nkurlu et al., 2020; Zhang et al., 2021).

Deep learning (DL) is a branch of ML and has already been researched in many different applications (Pilz et al., 2020). Deep neural networks (DNN) are a data-driven technology in DL that can establish complex nonlinear mapping relationships between inputs and outputs, which has led to extensive applications in fields such as oil and gas exploration. Compared to traditional ML methods, DL models, especially DNNs, can automatically extract complex features from raw data. This means that they can discover important patterns and relationships in the data without manual feature engineering. In addition, DL models have strong generalization capabilities that enable them to learn complex patterns and relationships in the data and perform well on new data (Najafabadi et al., 2015). For example, You et al. (2020) use a DNN model based on the Hudson-Cheng forward model (Cheng, 1993) to generate a large amount of training data, inverting shale anisotropy. Xiong et al. (2021) utilized Biot theory and DNNs to train elastic parameters of the wave propagation equation using logging data, establishing a DNN-based Biot theory for predicting seismic properties of shale oil reservoirs. In terms of permeability prediction, Qadrouh et al. (2019) provide guidance on ML, including petrophysical log prediction. They employed a neural network (NN) to link the density, sonic, gamma ray and neutron porosity logs to permeability. Synthetic data were generated using a theoretical model developed by Carcione et al. (2000) for training and testing. The tight reservoirs in the Chang 7 Member of the Ordos Basin host significant oil and gas resources and have recently become the main focus of unconventional hydrocarbon exploration and development. Current permeability mapping research in this region is mainly based on traditional permeability models or extended models based on laboratory measurements (Zhang et al., 2023). However, DNN has not yet

been used to predict permeability from of actual well logging data. Therefore, based on Qadrouh et al.'s research, a study on the log permeability of Chang 7 Member tight reservoir using DNNs is conducted in this work.

2. Study area and data

2.1. Overview of the study area

The Ordos Basin in western China is an extensive and stable polygenetic craton with a slightly westward tilted monocline (Guo et al., 2020). It can be divided into six different tectonic units, with the Tianhuan Depression and the Shanbei Slope being the most prominent units (Figure 1). These units also correspond to the regions with significant hydrocarbon deposits. In particular, the Shanbei Slope is the most important area for the distribution of Paleozoic natural gas and Mesozoic petroleum. Over time, beginning with the Late Triassic, the Ordos Basin transitioned to a lacustrine sedimentary environment in which the Upper Triassic Yanchang formation contains a series of fluvial-deltaic and lacustrine clastic rocks. The Yanchang formation can be divided into ten members, including the Chang 7 Member (Bai and Ma, 2020; Fang et al., 2022, 2024).

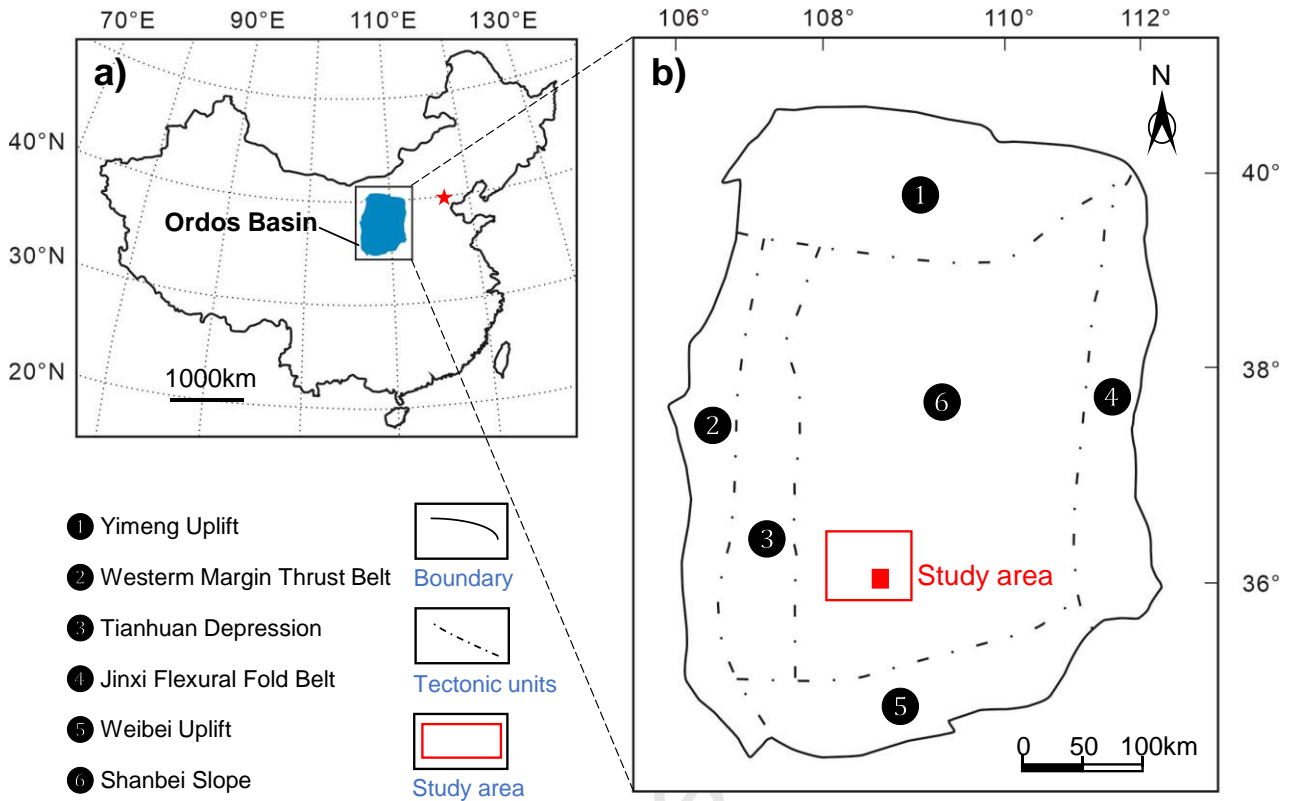
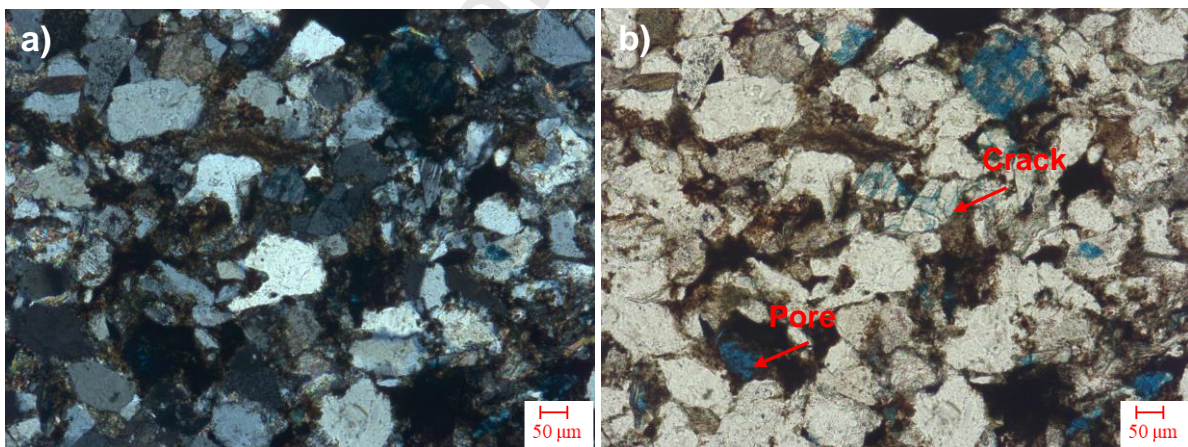


Figure 1. (a) Location of the Ordos Basin in China and (b) schematic geologic map of the basin.

The study area is located at the convergence point of the sediment sources in the southwest and northeast of the basin. The hydrocarbons in the tight sandstones and source rocks have not undergone long-distance migration and accumulation. They are defined as a variety of high-grade shale oils and tight oils and are especially abundant in the Changqing oil field. In recent years, the Chang 7 Member has emerged as an important exploration target. It can be subdivided from top to bottom into the Chang 7_1 , 7_2 and 7_3 layers. Chang 7_1 consists of mudstone interbedded with siltstone/sandstone and oil shale. Chang 7_2 consists of siltstone and fine sandstone locally interbedded with sandy siltstone, and thin layers of shale are also developed. Chang 7_3 consists mainly of black oil shale and siltstones (Fu et al., 2020).

As part of the preliminary investigations, we examined 21 rock samples from the study area. Figure 2 shows the thin sections of two most representative tight sandstone rocks examined in the laboratory. Figure 2a shows that the rock has a fine to silty sand structure. The detrital particles are predominantly fine to silty-sandy, well sorted and moderately round and belong to the fine to silty-lithic feldspathic sandstone. Figure 2c shows that the rock has a silty to fine sandy structure. The detrital particles are predominantly of fine sand size, well sorted and moderately round and belong to the silty to fine lithic feldspar sandstone. X-ray diffraction analysis shows that the main mineral components of the rock are quartz, feldspar and clay with a lower volumetric content of other minerals. Pores and cracks of different sizes can be observed (Figures 2b, d). The porosity and permeability of the rock samples were measured using the CMS-300 type overburden pressure porosity and permeability meter. As shown in Figure 3, the porosity is between 4.49 and 9.25%, while the permeability is between $10^{-17.3}$ and $10^{-16.1}$ m².



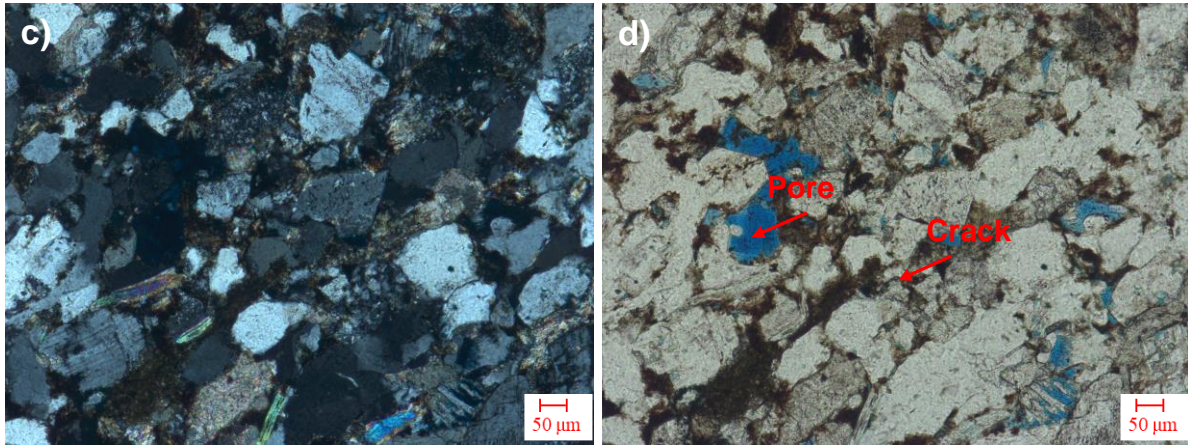


Figure 2. Thin sections of tight sandstone from the study area. Figures 2a, c show thin sections in cross-polarized light (XPL), and 2b and 2d in plane polarized light (PPL). The blue color corresponds to the pore space.

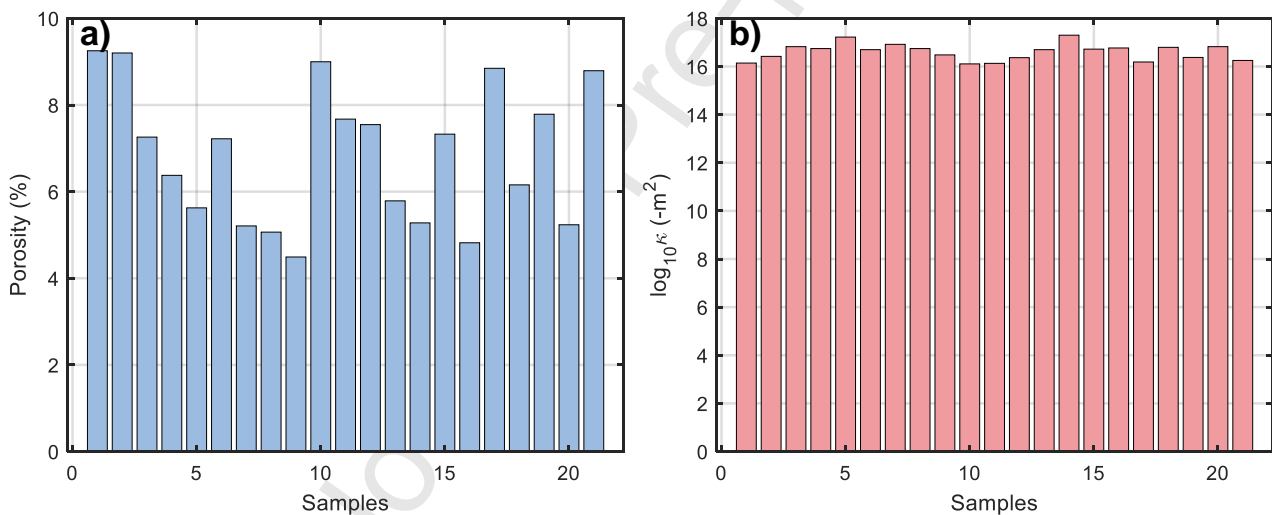


Figure 3. Porosity (a) and permeability (b) of the rock samples.

2.2. Data preparation

The dataset belong to 19 wells, which were processed and interpreted by the oilfield companies. After pre-processing the data, we obtained a total of 3783 data points from the reservoir sections of the wells. These data points are suitable for training and testing our models and include all required variables. The amount of data points may vary from well to well. To evaluate the model performance,

we selected two wells with enough data points as an independent test dataset. The remaining wells with 3037 data points were used to train the DNN model. Figure 4 shows the data from one of the wells, including S-wave and P-wave velocities (V_s and V_p), gamma ray (GR), resistivity (RT), impedance (I_p), density (ρ), permeability (κ), clay content (V_{cl}), porosity (ϕ), and Poisson's ratio (PR).

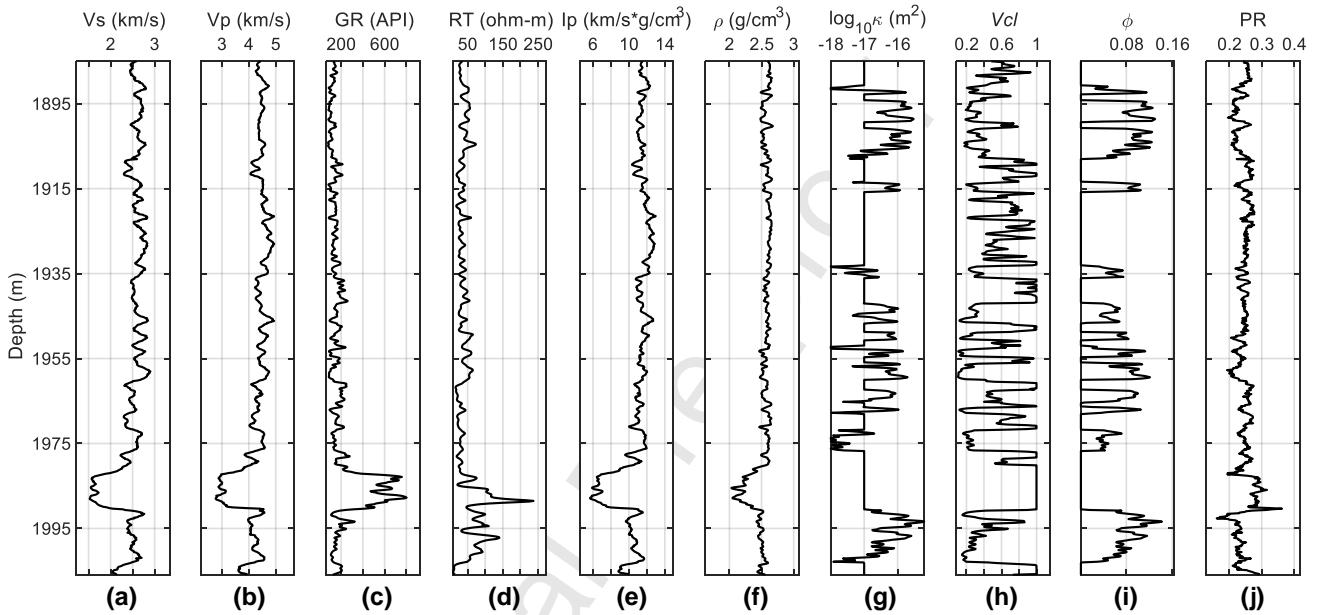


Figure 4. Well log data. (a) S-wave velocity, (b) P-wave velocity, (c) gamma ray, (d) resistivity, (e) impedance, (f) density, (g) permeability, (h) clay content, (i) porosity, and (j) Poisson's ratio.

3. Methodology

3.1. Deep neural networks

DNNs are networks with an input and output layer and at least one hidden layer in between. DNNs use sophisticated modelling in a complex way and can handle non-linear dependencies between different data sets. The performance of a DNN is strongly influenced by hyperparameters that must be specified in advance. Hyperparameters determine the structure of a DNN and how the network is trained. How to determine the optimal hyperparameters of a DNN model is an active area of research, but is outside the scope of our study. We determined these hyperparameters by trial and error. The

optimal DNN architecture is shown in Figure 5. We use a fully connected neural network and the input and output are $\mathbf{X}=(V_s, V_p, \rho, GR, RT, \phi, PR, Vcl, Ip)$ and κ , respectively. In between is a fully linked hidden layer, and each layer consists of ten units. In the NN, we choose the hyperbolic tangent function (tanh) as the activation function and use the adaptive moment estimation (Adam) algorithm as the optimization technique (Kingma and Ba, 2014). In training, we set 0.01 as the initial learning rate and choose the learning decay rate strategy. The learning process is based on the function 'lr_schedule', i.e. a function integrated in PyTorch that allows the learning rate to be adjusted as the number of epochs progresses (Paszke et al., 2017). In addition, the weights and biases are continuously adjusted to minimize the loss function. This is the mean squared error (MSE), which quantifies the discrepancy between the DNN predictions and the provided labels.

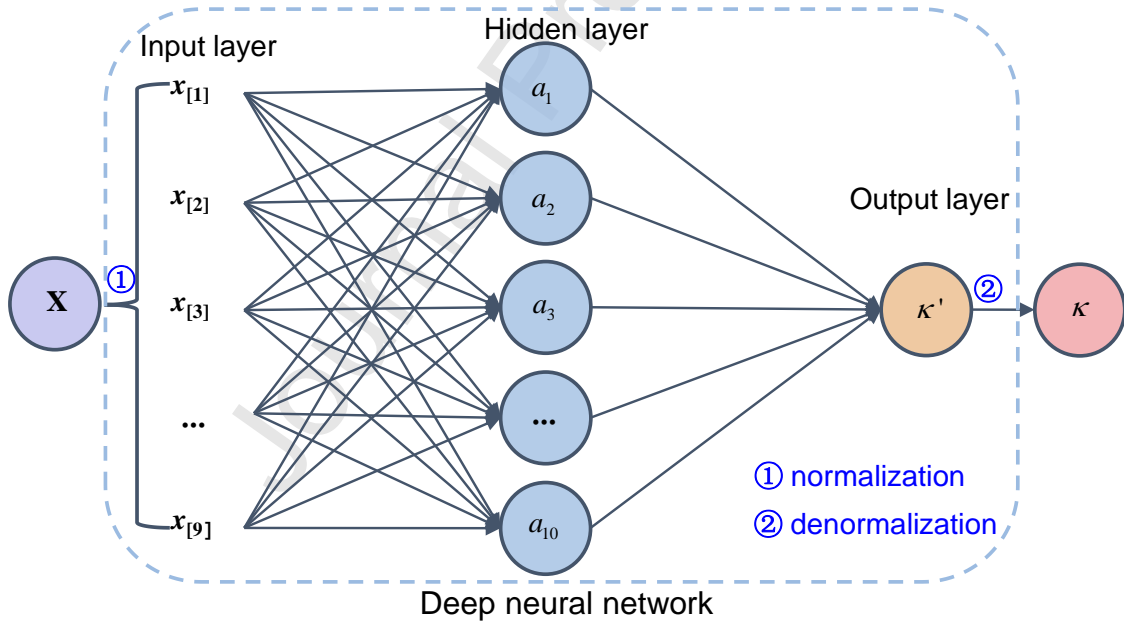


Figure 5. Schematic diagram of the deep neural network for permeability prediction.

It is crucial to normalize the data set, as each quantity varies greatly in unit and size, and the selection of the activation function also requires this action. In addition, data normalization helps to speed up convergence. The maximum and minimum values of the inputs, referred to as x_i^{\max} and x_i^{\min}

respectively, can be determined since \mathbf{X} is always available. One can use the mean and standard deviation of \mathbf{X} in the training dataset to normalize the input. Here x_i is normalized to $[-1, 1]$ by the following relationship:

$$x_i' = -1 + \frac{2}{x_i^{\max} - x_i^{\min}} (x_i - x_i^{\min}), \quad (1)$$

where $i = 1, 2, \dots, 9$.

It should be noted that the label κ is available when training the network, but the actual use of a well-trained DNN model is not. In this work, each label κ is normalized by dividing by 20. Therefore, when obtaining the prediction results, each label κ' is denormalized by multiplying by 20.

3.2. Evaluation metrics

The root-mean-squared error (RMSE) and R-squared (R^2) are used to quantitatively evaluate the accuracy of the predicted results:

$$\text{RMSE} = \sqrt{\frac{1}{n} \sum_{j=1}^n (\kappa_j^{\text{well}} - \kappa_j)^2}, \quad (2)$$

$$R^2 = 1 - \frac{\sum_{j=1}^n (\kappa_j^{\text{well}} - \kappa_j)^2}{\sum_{j=1}^n (\kappa_j^{\text{well}} - \bar{\kappa}_j^{\text{well}})^2}, \quad (3)$$

where n is the number of data points, κ_j^{well} denotes the j -th set of permeability of the real log data, κ_j denotes the j -th set of permeability of the DNN-based prediction, $\bar{\kappa}_j^{\text{well}} = \sum_{j=1}^n \kappa_j^{\text{well}} / n$ is the average. $R^2=1$

indicates that the DNN model performance is optimal.

4. Results

To train the DNN model, we consider 3783 data points from the reservoir sections of the 19 wells. The data from wells A and B (746 in total) are used to verify the performance of the DNN model and analyze the prediction accuracy. The loss value during the training process is shown in Figure 6a. It can be seen that the training loss gradually decreases and reaches a minimum value after 40,000 epochs. The convergence indicates that there is no overfitting and that the trained DNN model has reliable generalization capabilities. Figure 6b shows the comparison between the real and the calculated permeability values for the training set.

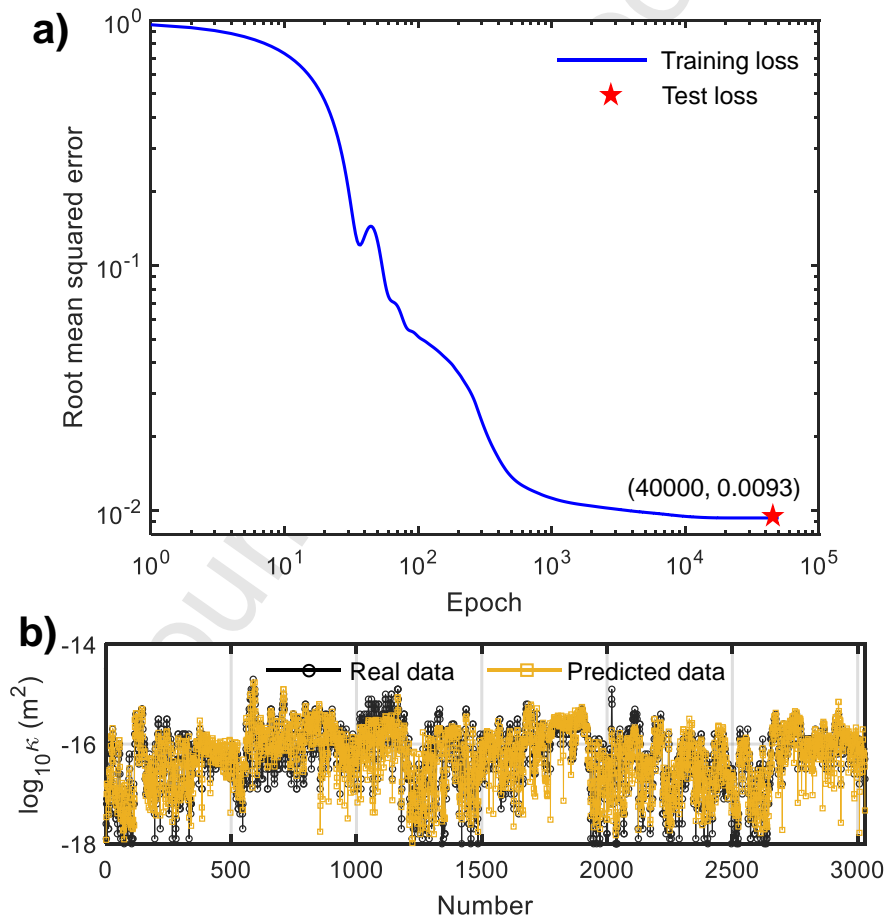


Figure 6. (a) Loss curve of a DNN model, and (b) results for the training set.

The comparison between the permeability predicted by the DNN model (blue curves) and the actual log data (black curves) are shown in Figures 7a and 8a. It can be seen that the prediction shows a good agreement with the real data. The relative errors of the predictions of the DNN model are

calculated (Figures 7b and 8b). The error is mainly within 5%. The distribution diagram of the relative error of the permeability for the two boreholes is shown in Figure 9. The prediction errors have a relatively narrow distribution, with average relative errors of 1.80% and 1.32% for wells A and B, respectively.

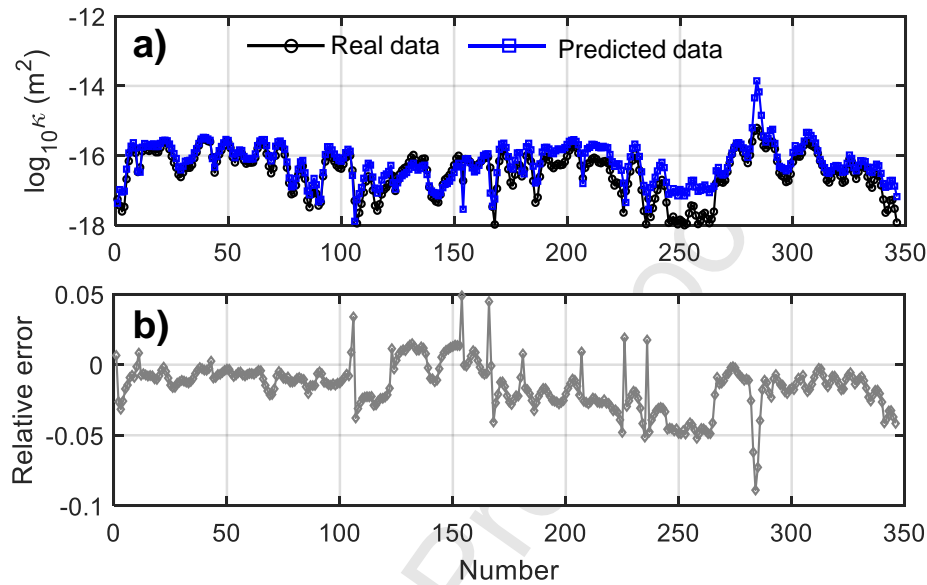


Figure 7. Permeability (a) and relative error (b) for well A.

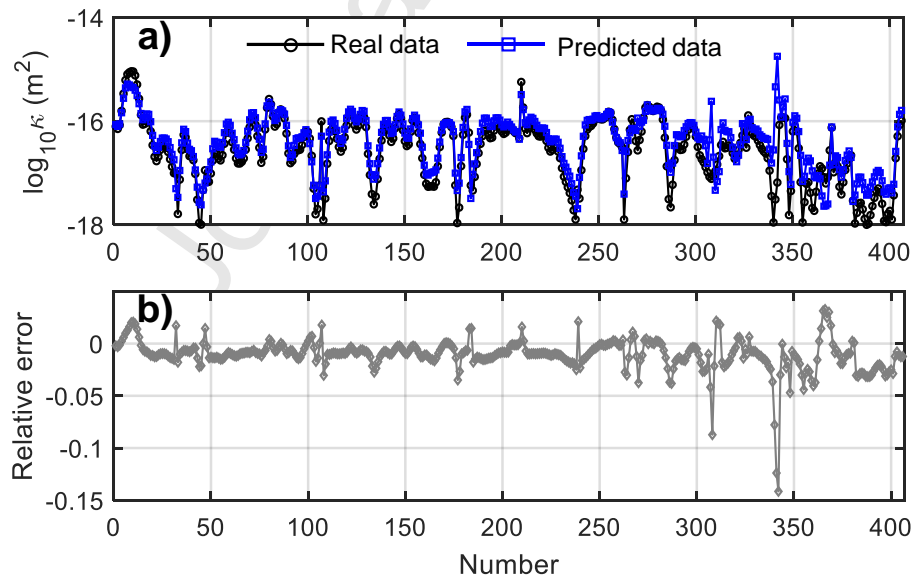


Figure 8. Permeability (a) and relative error (b) for well B.

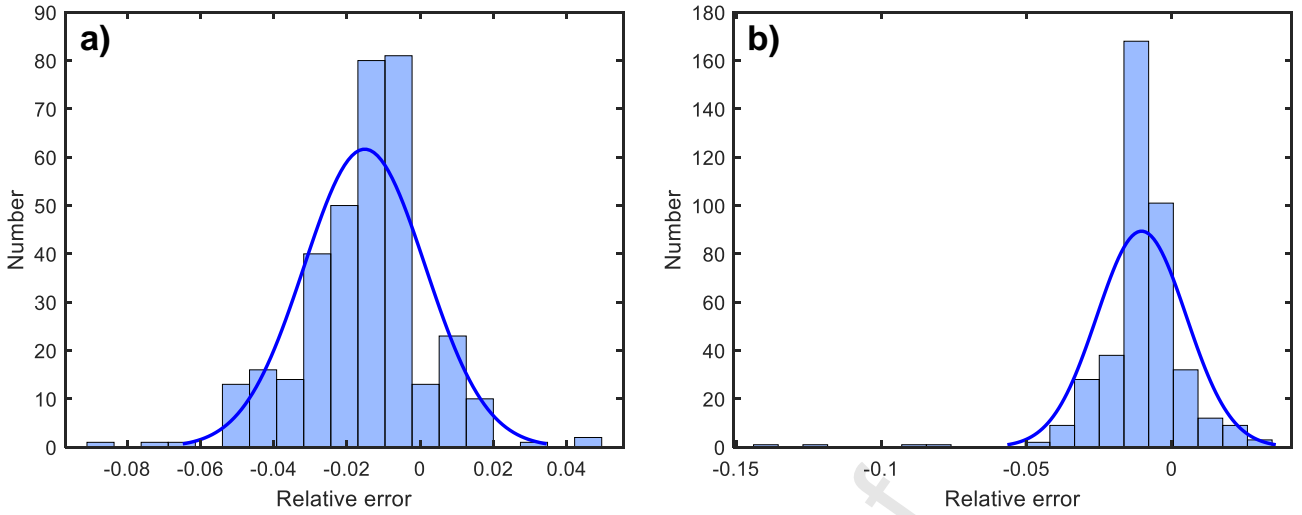


Figure 9. Errors for well A (a) and well B (b).

Table 1 lists the R^2 , relative RMSE and average relative error corresponding to the two wells.

Overall, the errors are small. A correlation analysis is performed to compare the results of the DNN model prediction with the real data. As can be seen in Figure 10, the prediction results correlate with the actual data, whereby the data scatter is mostly distributed close to the standard line.

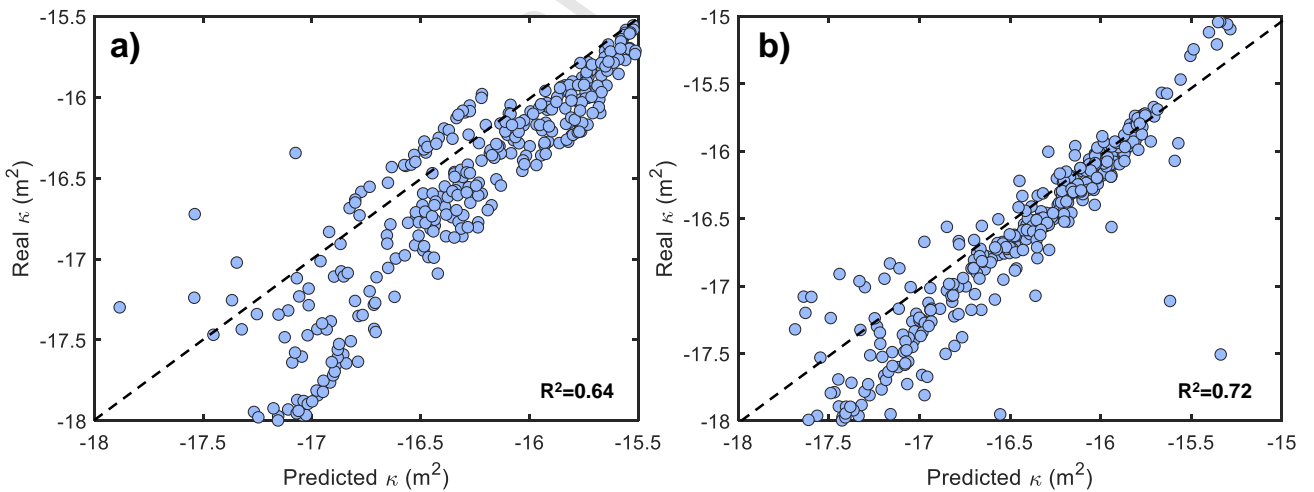
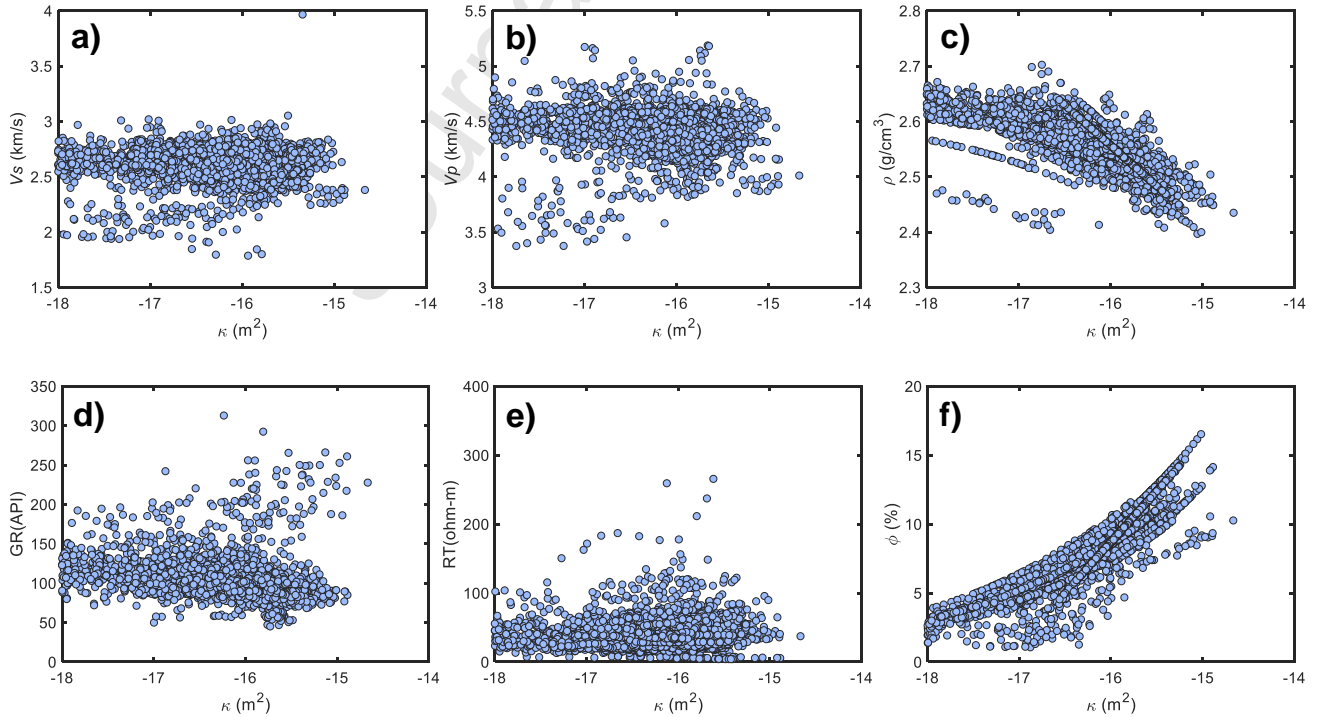


Figure 10. Crossplot of the real and predicted permeability by DNN model of nine inputs for well A (a) and well B (b).

Table 1. R^2 , relative RMSE, and average relative error between the log data and prediction results in Figures 7a and 8a.

Well	Evaluation metrics		
	R^2	Relative RMSE	Average relative error (%)
A	0.64	0.023	1.80
B	0.72	0.019	1.32

The nine inputs of the NN model were each analyzed against permeability, as shown in Figure 11. It can be seen that the correlations between the P- and S-wave velocities, resistivity and Poisson's ratio with permeability are relatively weak. Therefore, we chose new inputs to train the NN model. We use the same network architecture as mentioned above, where the inputs and outputs are denoted $\mathbf{X}' = (\rho, GR, \phi, Vcl, Ip)$ and κ , respectively. Figure 12 shows the comparison between the real and calculated permeability values for the training set.



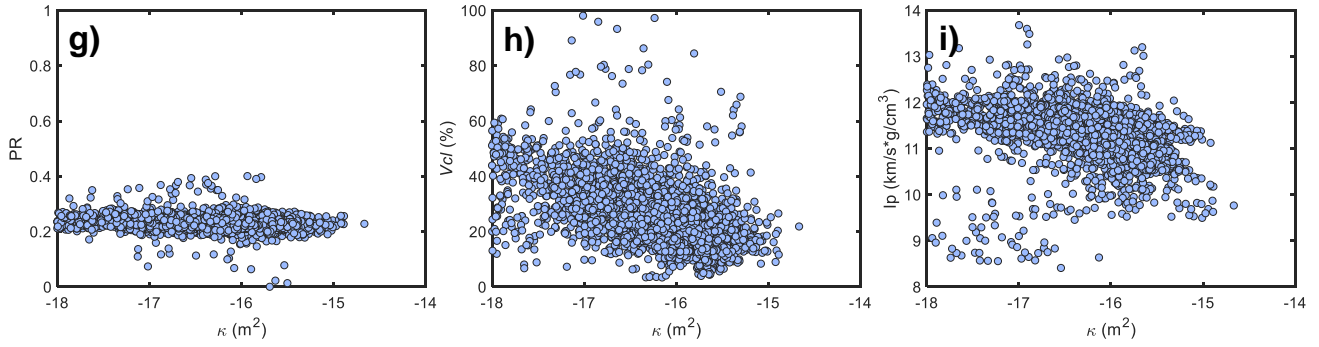


Figure 11. Crossplot of the permeability and S-wave velocity (a), P-wave velocity (b), density (c), gamma ray (d), resistivity (e), porosity (f), Poisson's ratio (g), clay content (h), and impedance (i).

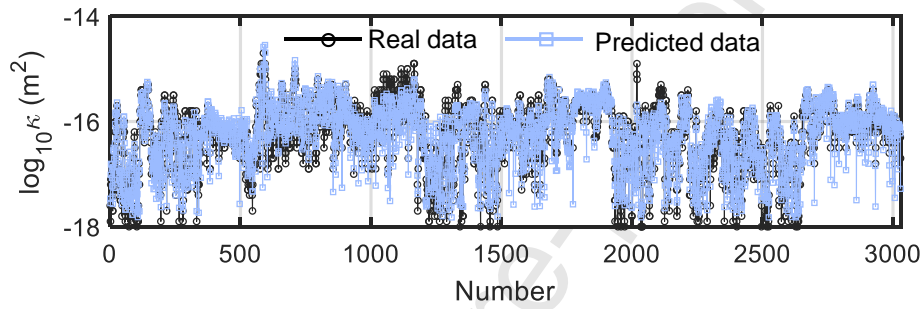


Figure 12. Results for the training set.

We used the trained network model to predict the permeability of wells A and B. The results are shown in Figures 13 and 14. It can be observed that the predicted results for both wells are in better agreement with the real data and have lower errors. As can be seen in Figure 15, the prediction errors have a relatively narrow distribution, with the average relative errors of 1.74% and 1.06% for wells A and B, respectively.

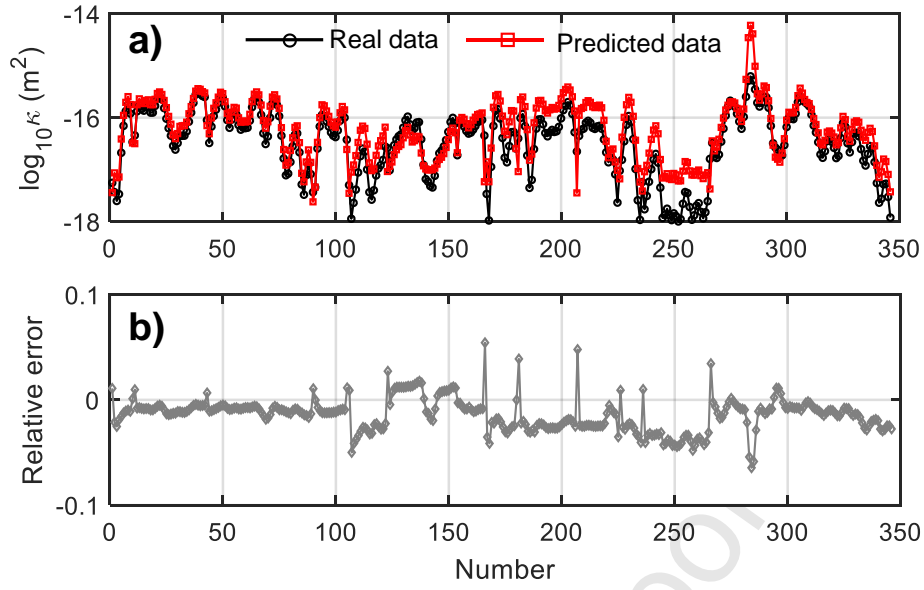


Figure 13. Permeability (a) and relative error (b) for well A.

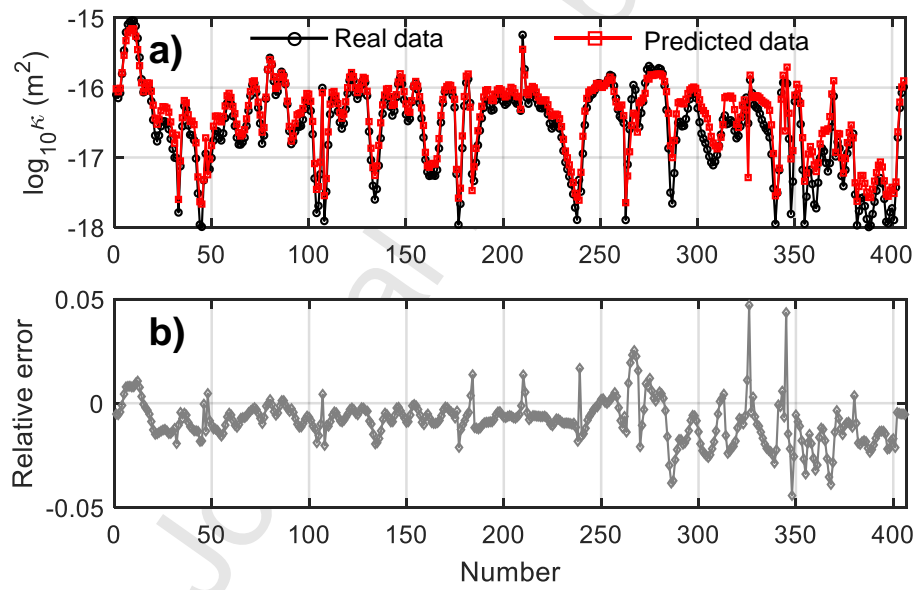


Figure 14. Permeability (a) and relative error (b) for well B.

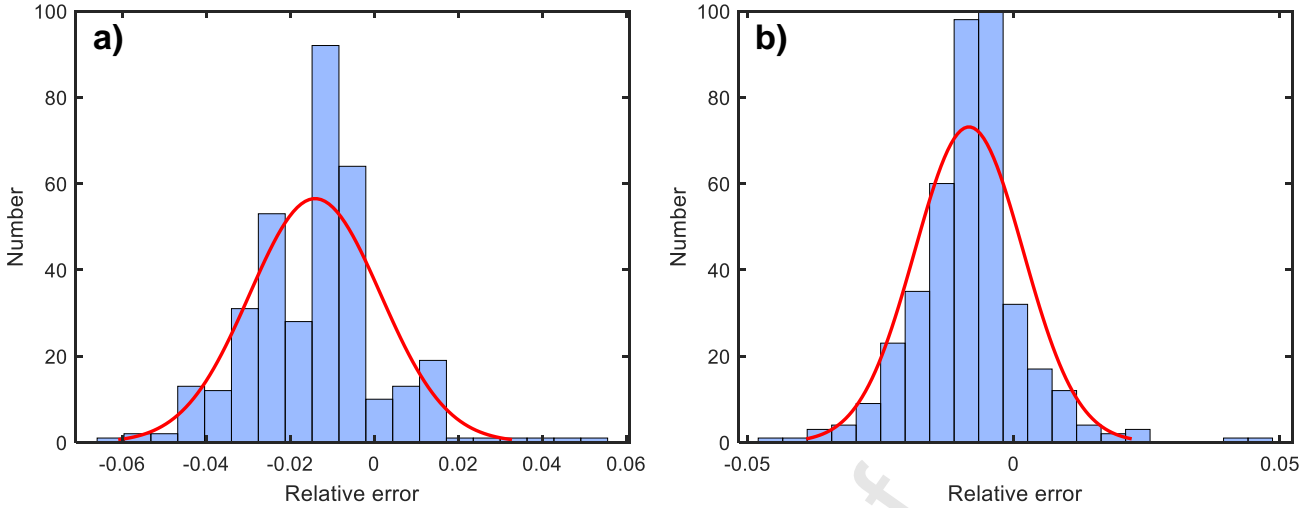


Figure 15. Errors for well A (a) and well B (b).

Table 2 lists the R^2 , relative RMSE and average relative error, corresponding to the two wells, for the newly-trained DNN model. As can be seen in Figure 16, the prediction results correlate with the actual data, with the data scatter mostly close to the standard line. A comparison of Table 1 and Table 2 shows that the newly-trained model has improved the prediction accuracy for wells A and B by reducing the input parameters of the DNN model and selecting parameters that are highly correlated with permeability.

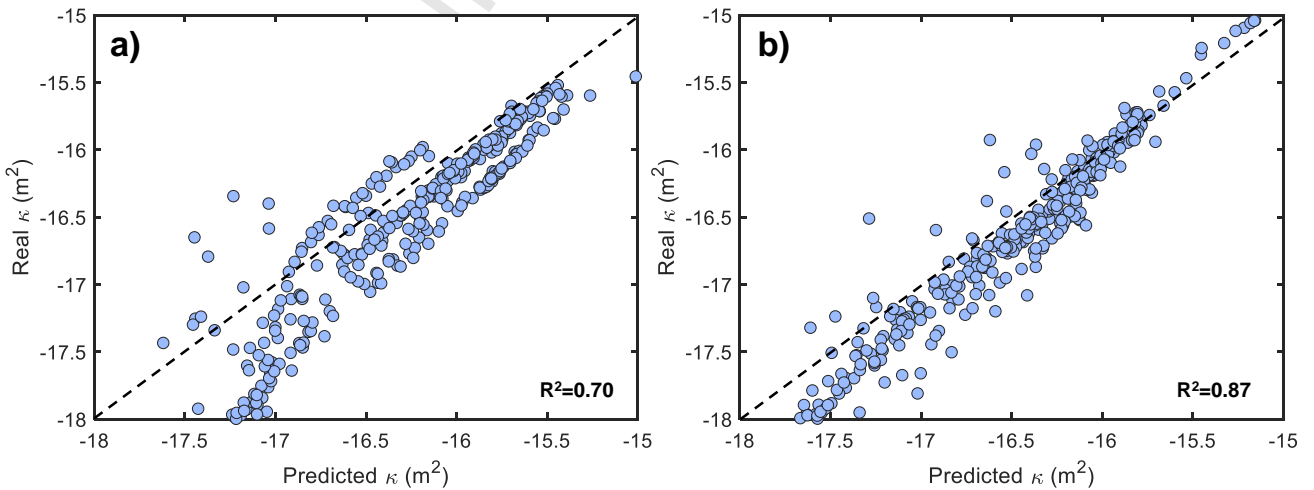


Figure 16. Crossplot of the real and predicted permeability by DNN of 5 inputs for well A (a) and well B (b).

Table 2. R^2 , relative RMSE, and average relative error between the log data and prediction results in Figures 13a and 14a.

Well	Evaluation metrics		
	R^2	Relative RMSE	Average relative error (%)
A	0.70	0.021	1.74
B	0.87	0.013	1.06

5. Discussion

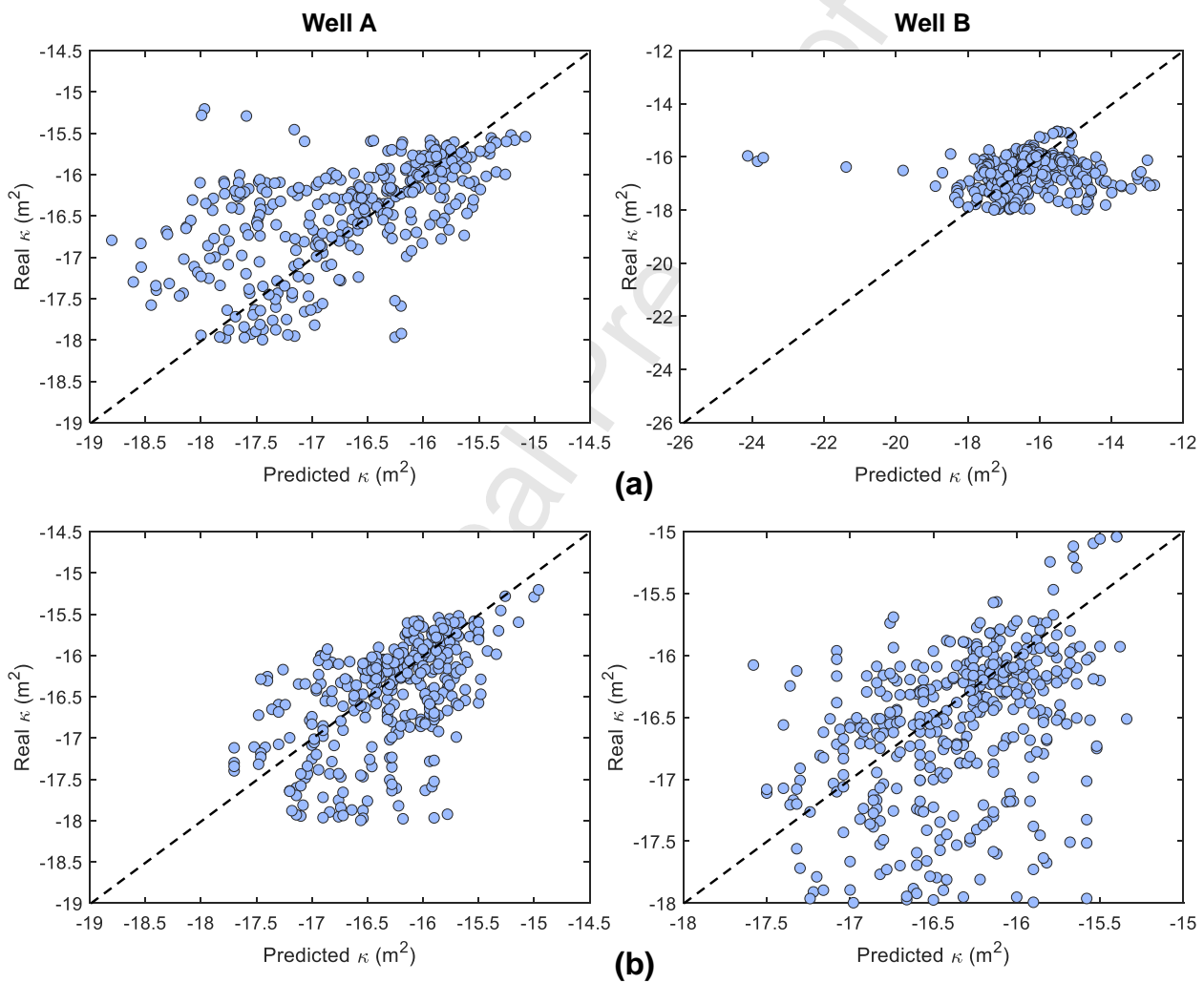
This part primarily compares the DNN-based permeability prediction method proposed in this work with current ML-based methods, emphasising the advantages of the proposed method. In addition, the generalizability of the proposed method is tested using log data from different regions.

5.1. Comparison with common ML-based methods

As mentioned in the Introduction, BP neural networks, KNN, XGBoost, DT and RF regression are the most common ML methods for simulating the intrinsic relationships between logging parameters and permeability. Therefore, the above common ML methods are used separately to predict permeability for wells A and B, with the data set, inputs and outputs matching the prediction processes shown in Figures 13 and 14. The results are shown in Figure 17. It can be seen from Figures 17a and b that the permeability prediction for wells A and B using the BP and KNN methods show significant deviations from the real data. The average relative errors for the predictions of well A are 3.23 % and 2.73 %, respectively, while the average relative errors for the predictions of well B are 5.19 % and 2.86 % for BP and KNN, respectively. As can be seen in Figures 17c to 17e, the prediction results correlate with the actual data, with the data scatter mostly close to the standard line. The average relative errors for the predictions of well A are 2.16%, 1.91% and 1.83%, respectively, while the average relative

errors for the predictions of well B are 1.21%, 1.29% and 1.15% for XGBoost, DT and RF, respectively. The errors are all larger than the method proposed in this work.

Comparing the prediction errors in Figures 17c and d, it can be seen that the error of DT for well A is lower than that of XGBoost, while the opposite is the case for well B. This also indicates that DL models have stronger generalization capabilities compared to traditional ML methods, resulting in better performance on new data.



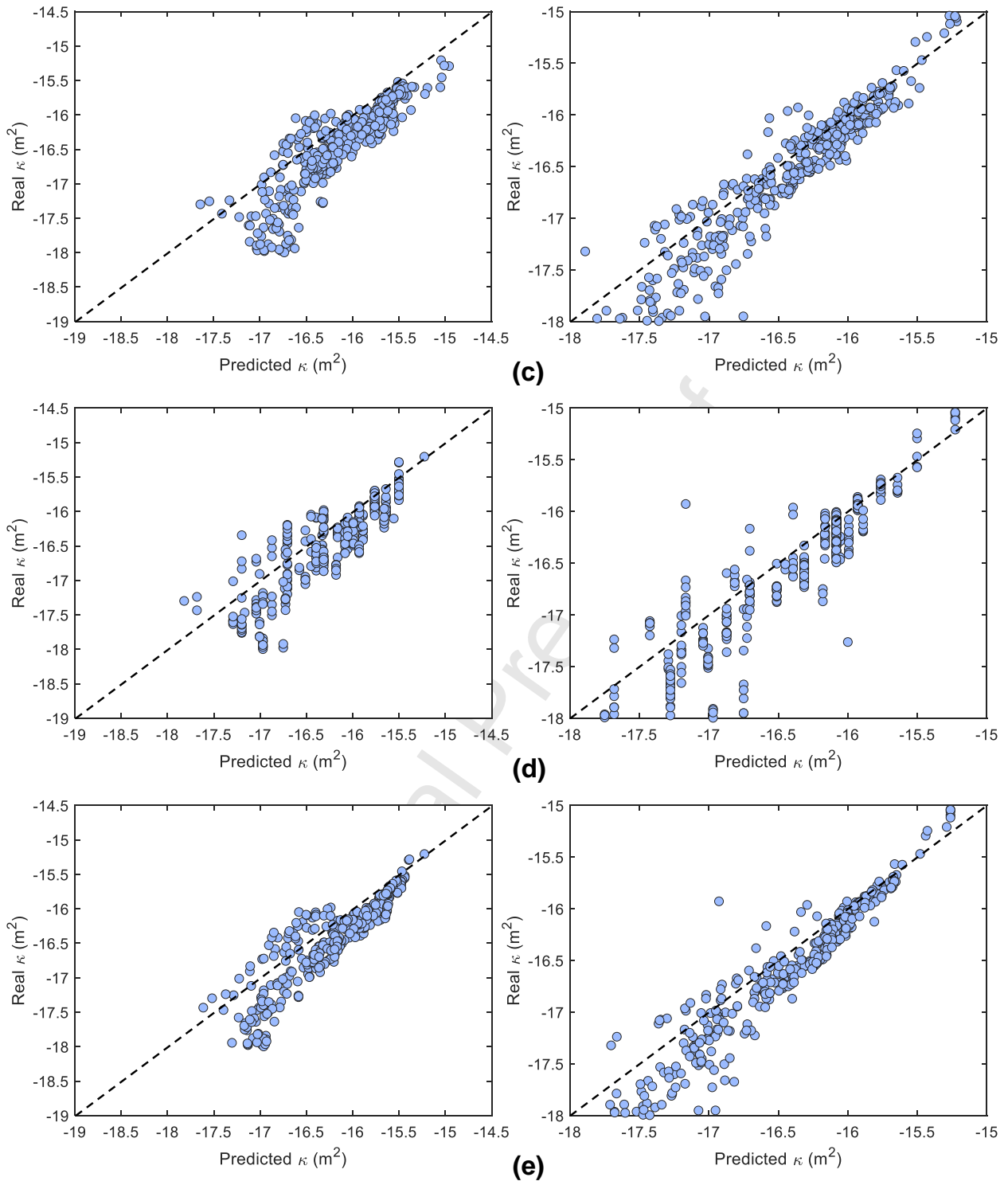


Figure 17. Crossplot of the real and predicted permeability by the different ML-based models: (a) BP, (b) KNN, (c) XGBoost, (d) DT, and (e) RF.

5.2. Generalizability of the proposed method

To illustrate the general aspects of the proposed method, log data from a tight-gas sandstone reservoir are selected to train the networks. The data are from the Sulige gas field, Ordos Basin, China. It includes 1704 data points with ρ , GR , ϕ , V_{cl} , I_p and κ . The dataset consists of 5 wells. To evaluate the performance of the model, we selected one well (well C) as an independent test dataset. The remaining wells with 1338 data points were used to train the DNN model. We use the same network architecture as mentioned above, where the inputs and outputs are $(\rho, GR, \phi, V_{cl}, I_p)$ and κ , respectively.

The results are shown in Figure 18. It can be observed that the predicted results for well C are in better agreement with the real data and have lower errors. The relative RMSE for the permeability predictions is 0.032, with an R^2 value of 0.75. As can be seen in Figure 19a, the prediction errors have a relatively narrow distribution with an average relative error of 1.91 %, and Figure 19b shows that the prediction results correlate with the actual data, with the data mostly scattering close to the standard line. The previous examples mainly focus on a shale/tight oil reservoir, while the example in this subsection shows that the proposed method can also be used for a tight-gas sandstone reservoir. These examples show that the DNN-based permeability prediction method in this work can provide high accuracy and general applicability.

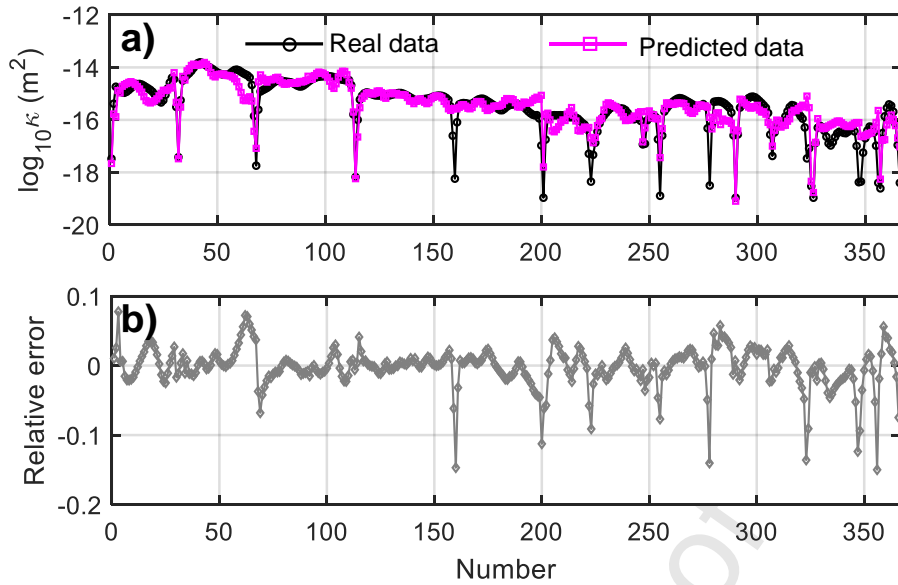


Figure 18. Results (a) and the relative error (b) for well C.

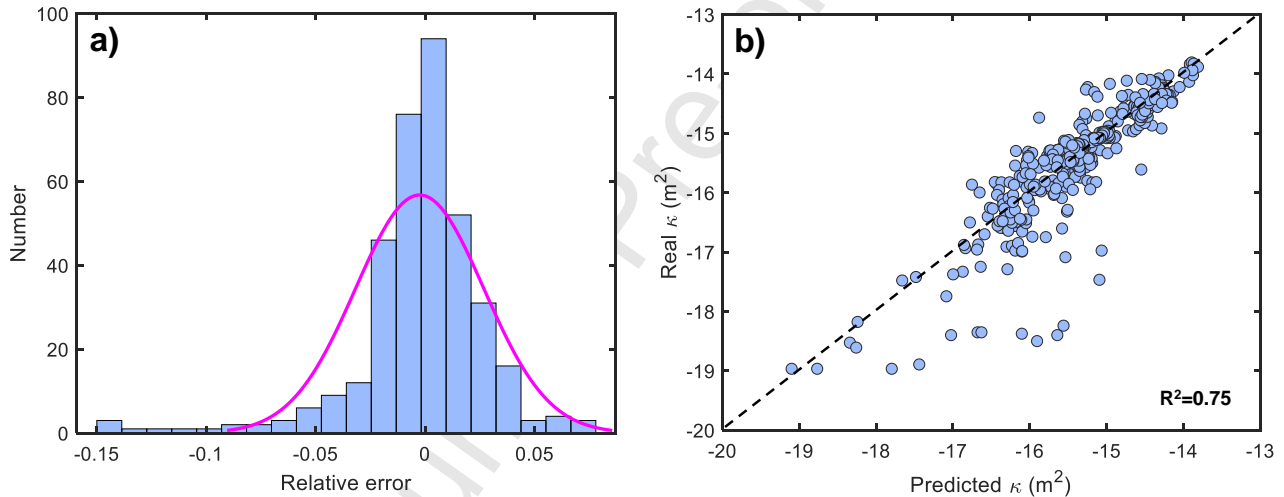


Figure 19. Errors (a) and crossplot (b) of the real and predicted permeability for well C.

6. Conclusions

In this work, permeability prediction studies were carried out in the tight reservoirs of the Chang 7 Member in the Ordos Basin based on a deep neural network. Data from 19 wells in the study area were used to train and test the network. First, the borehole data were pre-processed, resulting in 3783 valid data points. Two wells with many data points were selected for permeability prediction. The obtained parameters were used as inputs for the network, while the permeability data served as output.

After normalizing the data, the network was trained. The permeability prediction results for the two boreholes agreed well with the actual data with R^2 values of 0.64 and 0.72 (1 is optimal). We then performed a correlation analysis between the inputs and permeability and selected parameters that correlated strongly with permeability as new inputs to the network. Keeping the structure (with the same hyperparameters), we retrained the network. The new R^2 values were 0.70 and 0.87. Compared with conventional ML methods, the method proposed in this work provides more accurate and reliable permeability prediction. In addition, the prediction for different regions show that the proposed method has certain generalization capabilities and provides a technical approach to evaluate the sweet spots of tight reservoirs.

Acknowledgements

This work was supported by the Postgraduate Research & Practice Innovation Program of Jiangsu Province (KYCX24_0886), the National Natural Science Foundation of China (42174161), the Fundamental Research Funds for the Central Universities (B240205030), and the Natural Science Foundation of Jiangsu Province (BK20220995).

References

- Ahmed, U., Crary, S.F., Coates, G.R., 1991. Permeability estimation: The various sources and their interrelationships. *J. Pet. Technol.* 43(5), 578–587. <https://doi.org/10.2118/19604-PA>.
- An, W.Q., Yue, X.A., Zou, J.R., Zhang, L.J., Yan, R.J., 2023. Measuring gas permeability in tight cores at high pressure: Insights into supercritical carbon dioxide seepage characteristics. *Geoenergy Sci. Eng.* 229, 212070. <https://doi.org/10.1016/j.geoen.2023.212070>.
- Anemangely, M., Ramezanzadeh, A., Tokhmechi, B., 2017. Shear wave travel time estimation from

petrophysical logs using ANFIS-PSO algorithm: A case study from Ab-Teymour Oilfield. *J. Nat. Gas. Sci. Eng.* 38, 373–387. <https://doi.org/10.1016/j.jngse.2017.01.003>.

Archie, G.E., 1942. The electrical resistivity log as an aid in determining some reservoir characteristics. *Transactions of the AIME* 146(1), 54–62. <https://doi.org/10.2118/942054-G>.

Ba, J., Fang, Z.J., Fu, L.Y., Xu, W.H., Zhang, L., 2023a. Acoustic wave propagation in a porous medium saturated with a Kelvin–Voigt non-Newtonian fluid. *Geophys. J. Int.* 235, 2056–2077. <https://doi.org/10.1093/gji/ggad355>.

Ba, J., Zhu, H.S., Zhang, L., Carcione, J.M., 2023b. Effect of multiscale cracks on seismic wave propagation in tight sandstones. *J. Geophys. Res. Solid Earth* 128, e2023JB027474. <https://doi.org/10.1029/2023JB027474>.

Bai, Y.L., Ma, Y.H., 2020. Geology of the Chang 7 Member oil shale of Yanchang Formation of the Ordos Basin in central north China. *Pet. Geosci.* 26(2), 355–371. <https://doi.org/10.1144/petgeo2018-091>.

Bergen, K.J., Johnson, P.A., De Hoop, M.V., Beroza, G.C., 2019. Machine learning for data-driven discovery in solid earth geoscience. *Science* 363(6433), eaau0323. <https://doi.org/10.1126/science.aau0323>.

Botterill, T.E., McMillan, H.K., 2023. Using machine learning to identify hydrologic signatures with an encoder–decoder framework. *Water Resour. Res.* 59, e2022WR033091. <https://doi.org/10.1029/2022WR033091>.

Carcione, J.M., Gei, D., Yu, T., Ba, J., 2019. Effect of clay and mineralogy on permeability. *Pure Appl. Geophys.* 176, 2581–2594. <https://doi.org/10.1007/s00024-019-02117-3>.

Carcione, J.M., Gurevich, B., Cavallini, F., 2000. A generalized Biot-Gassmann model for the

acoustic properties of shaley sandstones. *Geophys. Prospect.*, 48, 539–557.

<https://doi.org/10.1046/j.1365-2478.2000.00198.x>.

Carcione, J.M., Poletto, F., Farina, B., Bellezza, C., 2018. 3D seismic modeling in geothermal reservoirs with a distribution of steam patch sizes, permeabilities and saturations, including ductility of the rock frame. *Phys. Earth Planet. Inter.* 279, 67–78.

<https://doi.org/10.1016/j.pepi.2018.03.004>.

Carcione, J.M., Qadrouh, A.N., Alajmi, M., Alqahtani, N.B., Ba, J., 2023. Rock acoustics of CO₂ storage in basalt. *Geophys. J. Int.* 234(3), 2429–2435. <https://doi.org/10.1093/gji/ggad252>.

Carman, P.C., 1961. *L'écoulement des gaz à Travers les milieux poreux*, Bibliothèque des Sciences et Techniques Nucléaires. Presses Universitaires de France.

Cheng, C.H., 1993. Crack models for a transversely isotropic medium. *J. Geophys. Res. Solid Earth* 98(B1), 675–684. <https://doi.org/10.1029/92JB02118>.

Fang, Z.J., Ba, J., Carcione, J.M., Liu, W.S., Wang, C.S., 2022. Estimation of the shear-wave velocity of shale-oil reservoirs: A case study of the Chang 7 Member in the Ordos Basin. *J. Seism. Explor.* 31, 81–104.

Fang, Z.J., Ba, J., Guo, Q., Xiong, F.S., 2024. Shear-wave velocity prediction of tight reservoirs based on poroelasticity theory: A comparative study of deep neural network and rock physics model. *Geoenergy Sci. Eng.* 240, 213028. <https://doi.org/10.1016/j.geoen.2024.213028>.

Fu, J.H., Li, S.X., Niu, X.B., Deng, X.Q., Zhou, X.P., 2020. Geological characteristics and exploration of shale oil in Chang 7 Member of Triassic Yanchang Formation, Ordos Basin, NW China. *Pet. Explor. Dev.* 47(5), 931–945.

[https://doi.org/10.1016/S1876-3804\(20\)60107-0](https://doi.org/10.1016/S1876-3804(20)60107-0).

- Guo, J.X., Gurevich, B., 2020. Frequency-dependent P wave anisotropy due to wave-induced fluid flow and elastic scattering in a fluid-saturated porous medium with aligned fractures. *J. Geophys. Res. Solid Earth* 125, e2020JB020320. <https://doi.org/10.1029/2020JB020320>.
- Guo, J.X., Gurevich, B., Chen, X.F., 2022. Dynamic SV-wave signatures of fluid-saturated porous rocks containing intersecting fractures. *J. Geophys. Res. Solid Earth* 127, e2022JB024745. <https://doi.org/10.1029/2022JB024745>.
- Guo, J.X., Liu, C., Abousleiman, Y.N., 2019. Transversely isotropic poroviscoelastic bending beam solutions for low-permeability porous medium. *Mech. Res. Commun.* 95, 1–7. <https://doi.org/10.1016/j.mechrescom.2018.11.001>.
- Guo, Q.L., Chen, X.M., Liuzhuang, X.X., Yang, Z., Zheng, M., Chen, N.S., Mi, J.K., 2020. Evaluation method for resource potential of shale oil in the Triassic Yanchang Formation of the Ordos Basin, China. *Energy Explor. Exploit.* 38(4), 841–866. <https://doi.org/10.1177/0144598720903394>.
- Guo, Z.Q., Nie, N.F., Liu, C., 2022a. Fracture characterization based on improved seismic amplitude variation with azimuth inversion in tight gas sandstones, Ordos Basin, China. *Mar. Pet. Geol.* 146, 105941. <https://doi.org/10.1016/j.marpetgeo.2022.105941>.
- Guo, Z.Q., Qin, X.Y., Liu, C., 2023. Quantitative characterization of tight gas sandstone reservoirs using seismic data via an integrated rock-physics-based framework. *Pet. Sci.* 20(6), 3428–3440. <https://doi.org/10.1016/j.petsci.2023.09.003>.
- Guo, Z.Q., Zhao, D.Y., Liu, C., 2022b. Gas prediction using an improved seismic dispersion attribute inversion for tight sandstone gas reservoirs in the Ordos Basin, China. *J. Nat. Gas. Sci. Eng.* 101, 104499. <https://doi.org/10.1016/j.jngse.2022.104499>.

- He, B., Xie, L.Z., Zhao, P., Ren, L., Zhang, Y., 2020. Highly efficient and simplified method for measuring the permeability of ultra-low permeability rocks based on the pulse-decay technique. *Rock Mech. Rock Eng.* 53 (1), 291–303. <https://doi.org/10.1007/s00603-019-01911-8>.
- Helle, H.B., Bhatt, A., Ursin, B., 2001. Porosity and permeability prediction from wireline logs using artificial neural networks: a North Sea case study. *Geophys. Prospect.* 49 (4), 431–444. <https://doi.org/10.1046/j.1365-2478.2001.00271.x>.
- Huang, Z., Shimeld, J., Williamson, M., Katsube, J., 1996. Permeability prediction with artificial neural network modeling in the Venture gas field, offshore eastern Canada. *Geophysics* 61 (2), 422–436. <https://doi.org/10.1190/1.1443970>.
- Jamshidian, M., Hadian, M., Zadeh, M.M., Kazempoor, Z., Bazargan, P., Salehi, H., 2015. Prediction of free flowing porosity and permeability based on conventional well logging data using artificial neural networks optimized by imperialist competitive algorithm-A case study in the South Pars Gas field. *J. Nat. Gas Sci. Eng.* 24, 89–98. <https://doi.org/10.1016/j.jngse.2015.02.026>.
- Kingma, D.P., Ba, J.L., 2014. Adam: a method for stochastic optimization. International Conference on Learning Representations (ICLR), San Diego, CA, USA.
- Lu, M.H., Han, T.C., Wang, P., Fu, L.Y., 2023. Permeability of artificial sandstones identified by their dual-pore structure. *Geophys. J. Int.* 234, 1422–1429. <https://doi.org/10.1093/gji/ggad149>.
- Madadi, M., Müller, T.M., 2019. Effect of porosity gradient on the permeability tensor. *Geophys. Prospect.* 69(3), 542–551. <https://doi.org/10.1111/1365-2478.12922>.
- Najafabadi, M.N., Villanustre, F., Khoshgoftaar, T.M., Seliya, N., Wald, R., Muharemagic, E., 2015. Deep learning applications and challenges in big data analytics. *J. Big Data* 2, 1.

<https://doi.org/10.1186/s40537-014-0007-7>.

- Nkurlu, B.M., Shen, C.B., Asante-Okyere, S., Mulashani, A.K., Chungu, J., Wang, L., 2020. Prediction of permeability using group method of data handling (GMDH) neural network from well log data. *Energies* 13(3), 551.
- Paszke, A., Gross, S., Chintala, S., Chanan, G., Yang, E., DeVito, Z., Lin, Z., Desmaison, A., Antiga, L., Lerer, A., 2017. Automatic differentiation in pytorch. 31st Conference on Neural Information Processing Systems (NIPS), Long Beach, CA, USA.
- Pilz, M., Cotton, F, Kotha, S.R., 2020. Data-driven and machine learning identification of seismic reference stations in Europe. *Geophys. J. Int.* 222(2), 861–873. <https://doi.org/10.1093/gji/ggaa199>.
- Qadrouh, A.N., Carcione, J.M., Alajmi, M., Alyousif, M.M., 2019. A tutorial on machine learning with geophysical applications. *Boll. Geofis. Teor. Applic.* 60(3), 375–402. <https://doi.org/10.4430/bgta0274>.
- Srisutthiyakorn, N., Mavko, G.M., 2017. What is the role of tortuosity in the Kozeny-Carman equation? *Interpretation* 5(1), SB57–SB67. <https://doi.org/10.1190/INT-2016-0080.1>.
- Timur, A., 1968. An investigation of permeability, porosity, & residual water saturation relationships for sandstone reservoirs. *Log Anal.* 9(4), 3–5.
- Xiong, F.S., Ba, J., Gei, D., Carcione, J.M., 2021. Data-driven design of wave-propagation models for shale-oil reservoirs based on machine learning. *J. Geophys. Res. Solid Earth* 126, e2021JB022665. <https://doi.org/10.1029/2021JB022665>.
- Xiong, F.S., Sun, W.T., Ba, J., Carcione, J.M., 2020. Effects of fluid rheology and pore connectivity on rock permeability based on a network model. *J. Geophys. Res. Solid Earth* 125(3),

e2019JB018857. <https://doi.org/10.1029/2019JB018857>.

You, N., Li, Y.E., Cheng, A., 2020. Shale anisotropy model building based on deep neural networks.

J. Geophys. Res. Solid Earth 125, e2019JB019042. <https://doi.org/10.1029/2019JB019042>.

Zhang, L., Gao, L., Ba, J., Zhang, M.B., Carcione, J.M., Liu, W.H., 2024. Permeability estimation of shale oil reservoir with laboratory-derived data: A case study of the Chang 7 Member in Ordos

Basin. *Appl. Geophys.* 21(1), 1–16. <https://doi.org/10.1007/s11770-024-1040-8>.

Zhang, Z., Zhang, H., Li, J., Cai, Z.X., 2021. Permeability and porosity prediction using logging data

in a heterogeneous dolomite reservoir: An integrated approach. *J. Nat. Gas. Sci. Eng.* 86, 103743. <https://doi.org/10.1016/j.jngse.2020.103743>.

Zhao, X.B., Chen, X.J., Huang, Q., Lan, Z.J., Wang, X.G., Yao, G.Q., 2022. Logging-data-driven permeability prediction in low-permeable sandstones based on machine learning with pattern

visualization: A case study in Wenchang A Sag, Pearl River Mouth Basin. *J. Petrol. Sci. Eng.* 214, 110517. <https://doi.org/10.1016/j.petrol.2022.110517>.

Declaration of Interest Statement

The authors declare that they have no known competing financial interests or personal relationships that could have appeared to influence the work reported in this paper.

The authors declare the following financial interests/personal relationships which may be considered as potential competing interests:

Journal Pre-proof

- DNN-based method is developed to predict permeability using logging data of tight reservoirs.
- Optimizing the input parameters by performing a crossplot analysis between input parameters and the permeability to improve prediction accuracy.
- The proposed method achieves satisfactory results in the practical applications for tight reservoirs.

Journal Pre-proof